Synthetic Metals 177 (2013) 105–109

Contents lists available at SciVerse ScienceDirect

Synthetic Metals

journal homepage: www.elsevier.com/locate/synmet

Letter

3-D ordered bimodal porous carbon/nickel oxide hybrid electrodes for supercapacitors

ARTICLE INFO

Keywords:
Nickel oxide
Supercapacitor
Activated carbon
Ordered carbon
Hybrid

ABSTRACT

3D-ordered bimodal porous carbons (3D-OBPCs) were fabricated, containing well-ordered macropores and a large amount of sub-/nanometer pores (micropores) with narrow pore size distribution. Nickel oxide (NiO) nanoparticles of 2–4 nm were introduced on the 3D-OBPCs. The 3D-OBPC/NiO nanoparticle hybrid exhibited better electrochemical performance than that of 3D-ordered macroporous carbon/NiO nanoparticle hybrid, because of the synergistic effects from the electric double-layer capacitance of a large amount of micropores, enhanced wettability due to oxygen heteroatoms introduced from the activation process, and pseudocapacitive redox reactions of NiO nanoparticles.

1. Introduction

Supercapacitors have attracted much attention for their high power capabilities, good reversibility, and long cycle life [1,2]. Supercapacitors are considered to be very attractive energy storage applications in various fields, such as electric vehicles, mobile phones, and uninterruptible power supplies for computers. However, at about 5 Wh/kg, the energy density of supercapacitors is lower than that of batteries, which has limited their adoption [1]. Therefore, it is important to enhance the energy density for such applications, which can be achieved by the development of advanced electrodes with high capacitance. To this end, nanostructure design and hybrid nanotechnology of electro-active components should be attained [3–5]. 3D-ordered macroporous carbons (3D-OMCs) with interconnected pore structures and highly developed porosity have potential for use in advanced electrodes for supercapacitors, because they can facilitate ion transport [6–9], and act as good catalyst supports due to their high surface area, favorable electrical properties, and open porous structure [10,11]. However, the electrodes for supercapacitors composed of only macroporous carbon-based materials have had low capacity. Therefore, more advanced strategies are required to achieve high capacitance in 3D-OMCs. The chemical activation of carbon-based materials can be used to develop a large amount of sub-/nanometer-scale pores, which can induce high electric double-layer capacitance (EDLC) by the pure electrostatic charge accumulated at the electrode/electrolyte interface and improved polar properties due to oxygen heteroatoms introduced from the activation process [9,12,13]. Also, various transition metal oxides such as ruthenium oxides, manganese oxides, and nickel oxides, have been developed as electrode materials with high capacitance by pseudocapacitive redox reactions [14–19]. Among them, nickel oxide has evident advantages of low cost and high theoretical capacity. Nonetheless, the high resistance of pure nickel oxide severely hinders its application.

In this study, 3D-ordered bimodal porous carbon (3D-OBPC), containing well-ordered macropores and a large amount of sub-/nanometer pores (micropores), was prepared using a colloidal crystal template method with a resorcinol-formaldehyde (RF) gel as a carbon precursor, and KOH as an activation agent. Also, nickel oxide (NiO) nanoparticles were incorporated on the carbon surface. The 3D-OBPC/NiO nanoparticle hybrid can exhibit high capacitance by synergistic effects from the EDLC of the large amount of sub-/nanometer pores, enhanced wettability due to oxygen heteroatoms induced by the activation process, and pseudocapacitive redox reactions of NiO nanoparticles. Furthermore, the ordered macropores of 3D-OBPCs can facilitate ion transport, and NiO nanoparticles can be homogeneously dispersed on the carbon surface with high electrical conductivity. Therefore, the electrochemical performance of the 3D-OBPC/NiO nanoparticle hybrid could be superior to those of 3D-OMC and 3D-OMC/NiO nanoparticle hybrids.

2. Experimental

2.1. Preparation of 3D-OBPCs

SiO_2 particles purchased from Alfa Aesar were dispersed in distilled water by ultrasonication. Then, 3D interconnected colloidal crystal template was obtained by a gravitational sedimentation method [20]. The template was sintered at 500 °C for 2 h to enhance the cohesion between the SiO_2 spheres. Next, RF carbon was synthesized according to an established method (Fig. 1(a)) [21]. Briefly, 1.23 g of resorcinol (99%, Sigma–Aldrich), 1.79 g of formaldehyde (37 wt% in water, Sigma–Aldrich), and 0.04 g of sodium carbonate (OCI company) were dissolved in 20 ml of distilled water, and mixed. Then, the SiO_2 template was immersed in this mixture and maintained for 6 h at room temperature. After the color of the solution changed to yellow, the SiO_2 template was extracted from the solution and thermally cured at 80 °C for 3 days to obtain cross-linked RF gel, which was confirmed by its

0379-6779/$ – see front matter © 2013 Elsevier B.V. All rights reserved.
http://dx.doi.org/10.1016/j.synthmet.2013.06.019

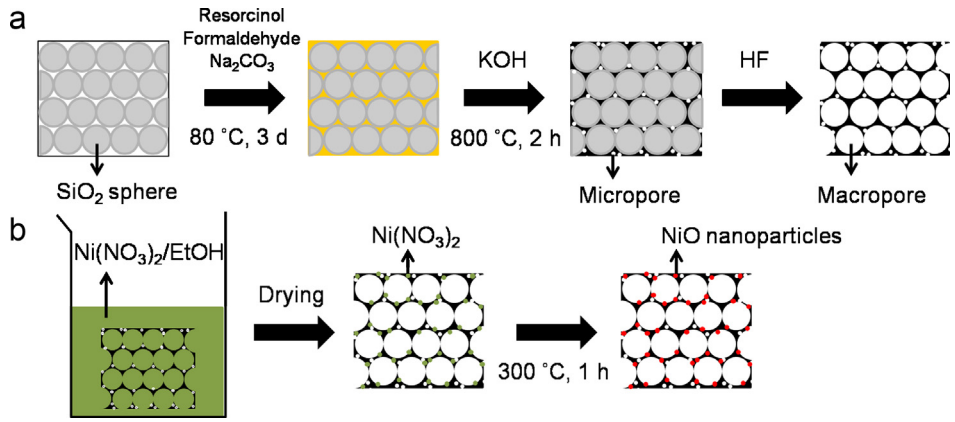

Fig. 1. (a) Schematic processing image of preparing (a) the 3D-OBPCs and (b) the 3D-OBPC/NiO nanoparticle hybrid.

dark red color. The SiO_2/RF gel was mixed with KOH at a 1:1 (w/w) ratio, and thermally treated at 800 °C with a holding time of 3 h, a heating rate of 5 °C/min, and a nitrogen flow of 200 ml/min for carbonization and activation. Then, the 3D-OBPCs were obtained after the removal of the silica microspheres by etching with 20 wt% hydrofluoric acid aqueous solution. The product was washed with distilled water and ethanol and dried in a vacuum oven.

2.2. Preparation of 3D-OBPC/NiO nanoparticle hybrid

Fig. 1(b) shows the schematic process for the 3D-OBPC/NiO nanoparticles. 20 wt% nickel nitrate was dissolved in ethanol, and the 3D-OBPCs were impregnated into the solution. The mixture was stirred for 6 h, so that $Ni(NO_3)_2$ was fully immersed in the pores of the 3D-OBPCs. After removing the solution, the sample was dried and then thermally treated at 300 °C for 1 h.

2.3. Characterization

The morphologies of the 3D-OBPCs were examined by scanning electron microscopy (SEM, S-4300, Hitachi, Japan). X-ray diffraction (XRD, Rigaku, DMAX-2500, Japan) was used to characterize the introduced NiO nanoparticles. Thermal gravimetric analysis (TGA, Q50, TA instruments, UK) of the samples was performed to determine the contents of NiO nanoparticles in the 3D-OBPC/NiO nanoparticle hybrid with a heating rate of 10 °C/min to 800 °C in air atmosphere. The microscopic morphology of the NiO nanoparticles on the surface of the 3D-OBPC was investigated by transmission

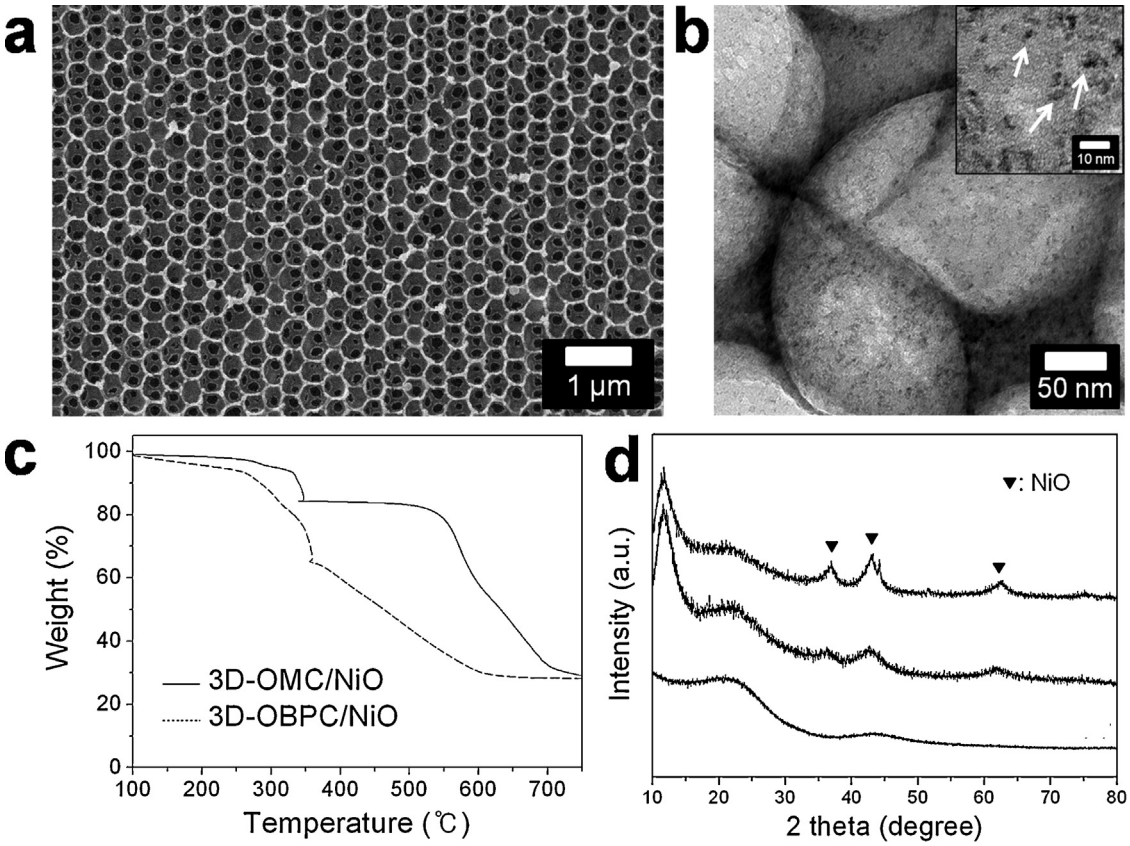

Fig. 2. (a) SEM image of the 3D-OBPCs and (b) TEM image of 3D-OBPC/NiO nanoparticle hybrid. (c) TGA data of the 3D-OMC/NiO and 3D-OBPC/NiO nanoparticle hybrids and (d) XRD data of 3D-OMC (bottom), 3D-OMC/NiO nanoparticle hybrid (middle) and 3D-OBPC/NiO nanoparticle hybrid (up).

Table 1
Textural properties, and carbon, oxygen, and nickel contents of the samples.

Sample name	S_{BET} ($m^2\ g^{-1}$)	S_{MIC} ($m^2\ g^{-1}$)	S_{EXT} ($m^2\ g^{-1}$)	Carbon (at%)	Oxygen (at%)	Nickel (at%)
3D-OMC	89.3	27.8	61.5	94.4	5.6	–
3D-OBPC	1402	1212.0	191.0	88.7	11.3	–
3D-OMC/NiO	95.0	20.5	74.5	76.9	17.6	5.5
3D-OBPC/NiO	1364.5	1182.2	182.3	70.4	24.1	5.5

electron microscopy (TEM, CM200, Philips, USA). XPS (PHI 5700 ESCA) analysis was performed using monochromated Al Kα radiation ($h\nu$ = 1486.6 eV). The Brunauer–Emmett–Teller (BET) specific surface area and pore diameter were measured using a nitrogen adsorption apparatus (ASAP 2020, Micromeritics, USA) at −196 °C.

2.4. Electrochemical characterization

The electrodes for the electrochemical tests were prepared as follows. The samples and polytetrafluoroethylene as a binder were mixed with a mass ratio of 9:1, coated onto a nickel mesh substrate (1 cm × 1 cm), and dried at 110 °C for several hours. Each electrode contained about 3–4 mg of the electroactive materials. All electrochemical measurements were performed in a three-electrode system. The samples containing nickel mesh, platinum plate, and saturated KCl were used as the working, counter, and reference electrodes, respectively. The measurements were carried out in a 2 M KOH solution at room temperature by a potentiostat/galvanostat (Autolab, PGSTAT302N, Netherlands). Cyclic voltammetry (CV) tests were performed between 0 and 0.5 V (vs. SCE) at different scan rates. The capacitance retentions were investigated at a scan rate of 50 mV/s for 1000 cycles.

3. Results and discussion

The 3D-OMCs, 3D-OMC/NiO nanoparticle hybrid, and 3D-OBPC/NiO nanoparticle hybrid were prepared through the process in Fig. 1. As shown in Fig. 2(a), a well-ordered macroporous carbon structure was obtained after removing the silica spheres, which were composed of macroporous spherical voids with diameters of 360 ± 30 nm. The TEM image shows that NiO nanoparticles of 2–4 nm were homogeneously dispersed on the surface of the 3D-OBPCs (Fig. 2(b)). The atomic ratios of the nickel on the 3D-OMC/NiO nanoparticle hybrid and the 3D-OBPC/NiO nanoparticle hybrid were calculated as 5.5% by XPS, which coincides with the result of TGA analysis (Fig. 2(c)). The crystal structures of the 3D-OMCs and NiO nanoparticles on the 3D-OMCs and 3D-OBPCs were investigated by XRD (Fig. 2(d)). The 3D-OMC shows two broad peaks at 22.3° and 43.4°, indicating an amorphous carbon structure. In the case of the 3D-OMC/NiO nanoparticle hybrid and the 3D-OBPC/NiO nanoparticle hybrid, there are three new peaks at 37.4°, 43.3°, and 62.8° corresponding to the (1 1 1), (2 0 0), and (2 2 0) diffraction planes related to the cubic structure of NiO [22]. From these results, we can confirm that the $Ni(NO_3)_2$ was completely changed to NiO according to the following equation:

$$Ni(NO_3)_2 \rightarrow Ni^{2+} + 2NO_3^-$$

$$Ni^{2+} + H_2O \rightarrow NiO(s) + 2H^+ \quad (1)$$

The pore structure of the 3D-OBPC/NiO nanoparticle hybrid was examined by measuring the nitrogen adsorption and desorption isotherms at 77 K using BET methods, as presented in Fig. 3. The isotherm curve exhibits IUPAC type-I shapes, indicating microporous structure induced by KOH activation [9,12,13]. The pore size distribution (PSD) of the 3D-OBPC/NiO nanoparticle hybrid shows that sub-nanometer pores below 8 Å were well-developed, and the PSD was very narrow (inset of Fig. 3). The surface area of the 3D-OBPC/NiO nanoparticle hybrid is 1364.5 $m^2\ g^{-1}$, which is more than 13 times the values of the non-activated samples (Table 1). Particularly, the surface area of the micropore range is 1182.2 $m^2\ g^{-1}$, indicating KOH activation induced mainly micropores in the sample. Therefore, the bimodal porous structure with very narrow PSD could be made by KOH activation of the 3D-OMC. Also, after KOH activation, oxygen heteroatoms were introduced in the 3D-OBPCs (Table 1). The 6.5 at% of oxygen atoms represented an increase in the 3D-OBPC/NiO nanoparticle hybrid compared to the 3D-OMC/NiO nanoparticle hybrid. This increased amount of oxygen atoms could be advantageous for the improvement of electrode wettability, which contributes to the expansion of the real electro-active surface area with the electrolyte.

The electro-chemical performance of the 3D-OMCs, 3D-OMC/NiO nanoparticle hybrid, and 3D-OBPC/NiO nanoparticle hybrid were analyzed in a 2 M KOH electrolyte (Fig. 4). The CV curves of 3D-OMC/NiO nanoparticle hybrid characterized at different scan rates show cathodic peaks around 0.35 V and an anodic peak around 0.2 V due to the pseudocapacitive effects of the NiO nanoparticles (Fig. 4(a)). The results are derived from the redox reaction of NiO and NiOOH in KOH electrolyte, which is described by the following equation:

$$NiO + OH^- \leftrightarrow NiOOH + e^- \quad (2)$$

The CV curves of the 3D-OBPC/NiO nanoparticle hybrid exhibit peaks similar to those of the 3D-OMC/NiO nanoparticle hybrid (Fig. 4(b). However, the electro-chemical double layer in the CV curves is thicker, and the peak is also larger than those of the 3D-OMC/NiO nanoparticle hybrid, indicating a relatively improved capacitance. The specific capacitance of the 3D-OMC/NiO nanoparticle hybrid was 357 F/g at a scan rate of 2 mV/s (Fig. 4(c)). This capacitance value is more than twice the value (168 F/g) of the 3D-OMCs. Also, the rate capabilities of the 3D-OMC/NiO nanoparticle hybrid at scan rates ranging from 2 to 100 mV/s are superior to those of the 3D-OMCs. At a scan rate of 100 mV/s, the capacitance value of the 3D-OMC/NiO nanoparticle hybrid

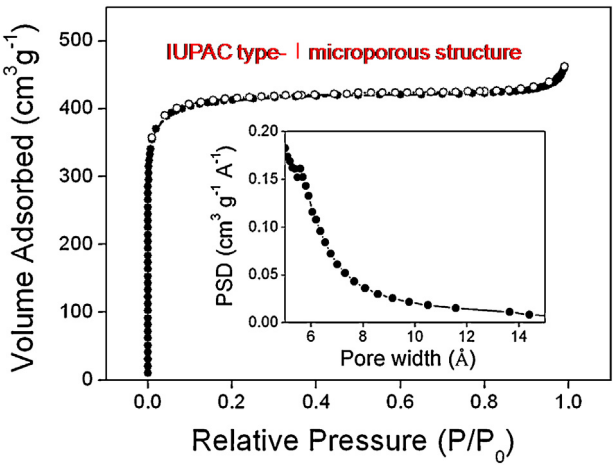

Fig. 3. Nitrogen adsorption and desorption isotherm curve and PSD (inset of Fig. 3) of 3D-OBPC/NiO nanoparticle hybrid.

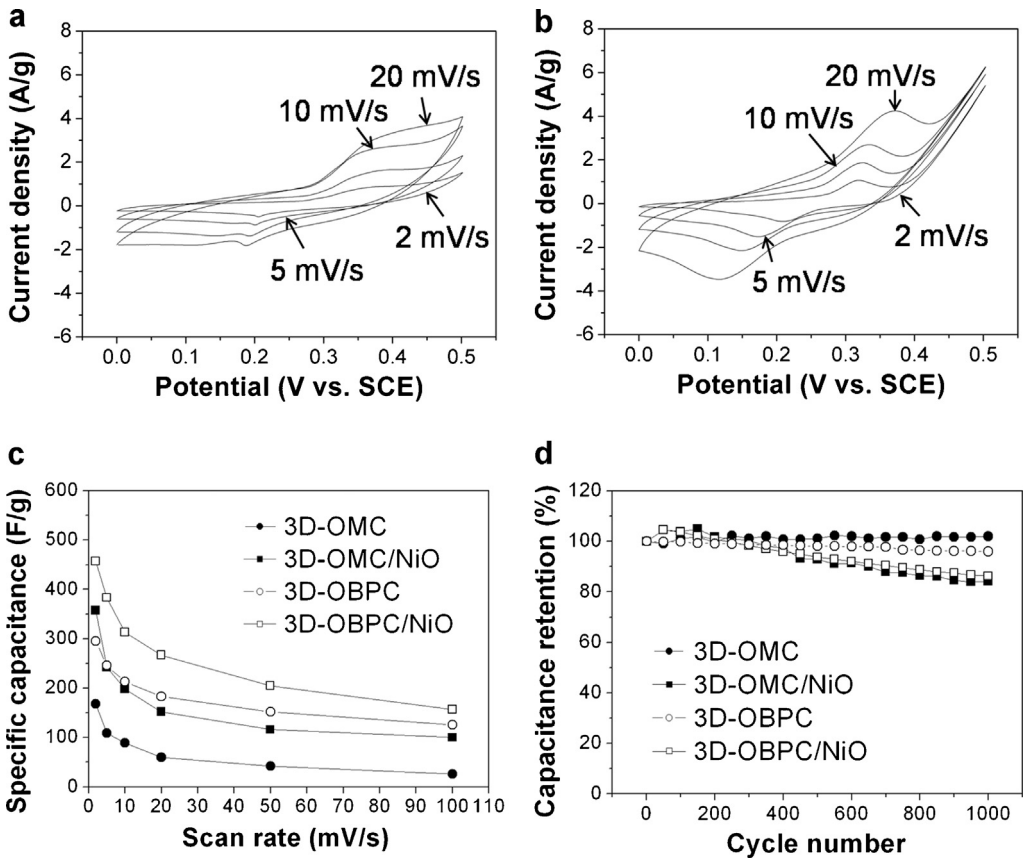

Fig. 4. Cyclic voltammograms of (a) 3D-OMC/NiO nanoparticle hybrid and (b) 3D-OBPC/NiO nanoparticle hybrid electrodes at different scan rates from 2 to 20 mV/s in 2 M KOH electrolyte. (c) Specific capacitances of 3D-OMC, 3D-OMC/NiO nanoparticle hybrid, 3D-OBPC and 3D-OBPC/NiO nanoparticle hybrid electrodes as a function of scan rates. (d) Cyclic stabilities of the 3D-OMC, 3D-OMC/NiO nanoparticle, 3D-OBPC and 3D-OBPC/NiO nanoparticle hybrid electrodes at a scan rate of 50 mV/s during 1000 cycles.

is more than threefold the value of the 3D-OMCs. These results suggest that heterogeneous hybrid system of electro-active components is more effective for the electro-chemical performance. In the case of 3D-OBPCs used as the electro-active component, the specific capacitance was 295 F/g, which is much higher than 168 F/g of the 3D-OMCs. The large amount of micorpores in the 3D-OBPCs highly contributed to an enhancement of the EDLC by providing large surface area for electrostatic charge storage. Furthermore, with incorporation of NiO nanoparticles on the surface of the 3D-OBPCs, the specific capacitance of 457 F/g was achieved at a scan rate of 2 mV/s, and a specific capacitance of *c.a.* 205 F/g could still be obtained at a scan rate of 50 mV/s. The high capacitance and rate capabilities of the 3D-OBPC/NiO nanoparticle hybrid surpass those of the 3D-OMC/NiO nanoparticle hybrid. The superior performances are induced by contributions of both EDLC and pseudocapacitance from NiO nanoparticles. These results were supported by galvanostatic discharge curves of the 3D-OBPC/NiO nanohybrid electrode. In the galvanostatic discharge curves, there are distinct plateaus by faradic reactions of nickel oxide, and also the curves exhibit diagonal slopes due to EDLC except the plateau regions (Fig. 5) Moreover, the plateau ratio on the total times for discharging is larger in the low current density than in the high current density. This result suggests that pseudocapacitive effects are effective on the relatively low current density. After 1000 cycles at a scan rate 50 mV/s, the capacitances of the 3D-OMC/NiO nanoparticle hybrid and 3D-OBPC/NiO nanoparticle hybrid were decreased to 16% and 14% of the initial capacitance, respectively, demonstrating that the hybrid electrodes have good cycle stabilities (Fig. 4(d)).

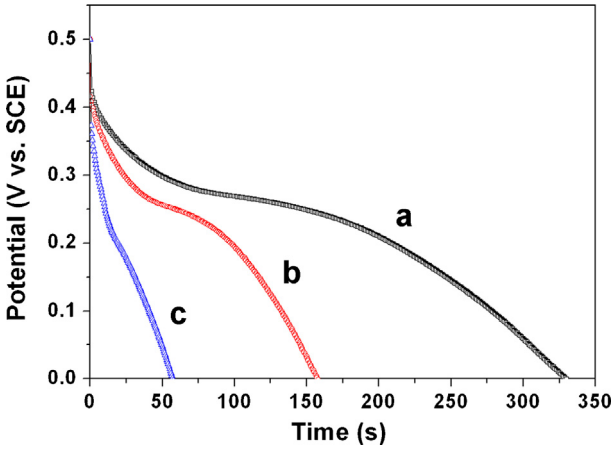

Fig. 5. Galvanostatic discharge curves of 3D-OBPC/NiO nanoparticle hybrid at different current densities ((a) 0.8 A/g, (b) 1.5 A/g and (c) 3 A/g). (For interpretation of the references to colour in this figure legend, the reader is referred to the web version of this article.)

4. Conclusions

3D-OMC, 3D-OMC/NiO nanoparticle hybrid, and 3D-OBPC/NiO nanoparticle hybrid were successfully prepared, and their electrochemical performance was investigated. The 3D-OMC/NiO nanoparticle hybrid exhibited enhanced capacitance compared to 3D-OMC due to the pseudocapacitive effects of the NiO nanoparticles. Also, a large amount of micropores in the 3D-OBPC/NiO nanoparticle hybrid contributed the further

enhancement of the capacitance by EDLC with the pseudo-capacitive effects of the NiO nanoparticles. The 3D-OBPC/NiO nanoparticle hybrid showed a capacitance of 457 F/g at a scan rate of 2 mV/s, and a specific capacitance of *c.a.* 205 F/g could still be obtained at a scan rate of 50 mV/s. Stable electro-chemical performance was maintained for 1000 cycles.

Acknowledgements

This work was supported by the National Research Foundation of Korea Grant funded by the Korean Government (MEST) (NRF-2010-C1AAA001-0029018), and also supported by Basic Science Research Program through the National Research Foundation of Korea (NRF) funded by the Ministry of Education (2013008534).

References

[1] P. Simon, Y. Gogotsi, Nature Materials 7 (2008) 845–854.
[2] J.R. Miller, P. Simon, Science 321 (2008) 651–652.
[3] A.S. Aricò, P. Bruce, B. Scrosati, J.-M. Tarascon, W.V. Schalkwijk, Nature Materials 4 (2005) 366–377.
[4] D.R. Rolison, J.W. Long, J.C. Lytle, A.E. Fischer, C.P. Rhodes, T.M. McEvoy, M.E. Bourg, A.M. Lubers, Chemical Society Reviews 38 (2009) 226–252.
[5] Z. Xu, Z. Li, C.M.B. Holt, X. Tan, H. Wang, B.S. Amirkhiz, T. Stephenson, D. Mitlin, Journal of Physical Chemistry Letters 3 (2012) 2928–2933.
[6] C. Vix-Guterl, E. Frackowiak, K. Jurewicz, M. Friebe, J. Parmentier, F. Béguin, Carbon 43 (2005) 1293–1302.
[7] L.L. Zhang, D. Li, J. Zhang, P. Guo, J. Zheng, X.S. Zhao, Chemistry of Materials 22 (2010) 1195–1202.
[8] J. Feng, J. Zhao, B. Tang, P. Liu, J. Xu, Journal of Solid State Chemistry 183 (2010) 2932–2936.
[9] Y.S. Yun, J. Shim, Y. Tak, H.-J. Jin, RSC Advances 2 (2012) 4353–4358.
[10] B. Fang, J.H. Kim, M. Kim, J.-S. Yu, Chemistry of Materials 21 (2009) 789–796.
[11] F. Su, X.S. Zhao, Y. Wang, J. Zeng, Z. Zhou, J.Y. Lee, Journal of Physical Chemistry B 109 (2005) 20200–20206.
[12] Y.S. Yun, S.Y. Cho, J. Shim, B.H. Kim, S.-J. Chang, S.J. Baek, Y.S. Huh, Y. Tak, Y.W. Park, S. Park, H.-J. Jin, Advanced Materials 25 (2013) 1993–1998.
[13] Y.S. Yun, C. Im, H.H. Park, I. Hwang, Y. Tak, H.-J. Jin, Journal of Power Sources 234 (2013) 285–291.
[14] Z.-S. Wu, D.-W. Wang, W. Ren, J. Zhao, G. Zhou, F. Li, H.-M. Cheng, Advanced Functional Materials 20 (2010) 3595–3602.
[15] X. Liu, P.G. Pickup, Journal of Power Sources 176 (2008) 410–416.
[16] S. Chen, J. Zhu, X. Wu, Q. Han, X. Wang, ACS Nano 4 (2010) 2822–2830.
[17] X. Xie, L. Gao, Carbon 45 (2007) 2365–2373.
[18] M.-S. Wu, C.-Y. Huang, K.-H. Lin, Journal of Power Sources 186 (2009) 557–564.
[19] B. Wen, S. Zhang, H. Fang, W. Liu, Z. Du, Materials Chemistry and Physics 131 (2011) 8–11.
[20] A. Esmanski, G.A. Ozin, Advanced Functional Materials 19 (2009) 1999–2010.
[21] S.-W. Woo, K. Dokko, H. Nakano, K. Kanamura, Journal of Materials Chemistry 18 (2008) 1674–1680.
[22] P. Azadi, R. Farnood, E. Meier, Journal of Physical Chemistry A 114 (2010) 3962–3968.

Young Soo Yun
Doo Jin Park
Min Jae Joo
Hyoung-Joon Jin*
Department of Polymer Science and Engineering, Inha University, Incheon 402-751, Republic of Korea

* Corresponding author. Tel.: +82 32 860 7483.
E-mail address: hjjin@inha.ac.kr (H.-J. Jin)

3 February 2013

21 June 2013

24 June 2013

Available online 18 July 2013